AIP | Journal of Applied Physics

Stochastic limits in synchronous imaging of sub-micron magnetization dynamics using scanning transmission x-ray microscopy

Cheng Cheng, Konstantine Kaznatcheev, and William E. Bailey

Citation: J. Appl. Phys. **111**, 07E321 (2012); doi: 10.1063/1.3673825
View online: http://dx.doi.org/10.1063/1.3673825
View Table of Contents: http://jap.aip.org/resource/1/JAPIAU/v111/i7
Published by the American Institute of Physics.

Stochastic limits in synchronous imaging of sub-micron magnetization dynamics using scanning transmission x-ray microscopy

Cheng Cheng,[1,a)] Konstantine Kaznatcheev,[2] and William E. Bailey[1]
[1]*Materials Science and Engineering Program, Department of Applied Physics and Applied Mathematics, Columbia University, New York, New York 10027, USA*
[2]*NSLS, Brookhaven National Lab, Upton, New York 11973, USA*

(Presented 2 November 2011; received 25 September 2011; accepted 31 October 2011; published online 28 February 2012)

We demonstrate a synchronous (lock-in) technique for imaging thin-film magnetization dynamics using scanning transmission x-ray microscopy (STXM). Gated photon counting synchronized with magnetic field modulation allows image acquisition with differential contrast for high and low magnetization. We have applied this technique to 5×12 μm^2 $Ni_{81}Fe_{19}$ ellipses with well-defined closure domains at remanence. The stochastic nature of the domain wall motion and nucleation is apparent in images recorded during cycling along successive major hysteresis loops. Synchronous imaging shows the clearest enhancement of contrast for small-amplitude domain wall motion, with a less obvious benefit at higher fields/displacements. The technique shows promise for the contrast enhancement of magnetization in dynamics in STXM. © *2012 American Institute of Physics*. [doi:10.1063/1.3673825]

I. INTRODUCTION

Magnetization dynamics of soft ferromagnetic thin-film patterned structures play a fundamental role in a wide range of applications, including, but not limited to, magnetic recording devices and emerging spintronic technology.[1–3] Recent research has focused on high frequency dynamics into the GHz range, driven by the demand for faster-operating devices.[4–6] However, low-frequency dynamics are also of interest for other devices such as integrated inductors, which operate at rates below 500 MHz.[7,8] Low-frequency dynamics are critical for analyzing the magnetic reversal and domain wall propagation processes. Time-resolved magnetic microscopy offers the potential to image the domain dynamics studied, to date, through other means.[9,10]

We have developed a technique to provide and ultimately enhance dynamic magnetic contrast in scanning transmission x-ray microscopy (STXM). The STXM is of increasing interest in magnetization dynamics studies because of its high, 15–40 nm spatial resolution, the ability to probe buried magnetic layers with elemental specificity, and the potential for temporal resolution due to the x-ray bunch structure at 3rd generation synchrotrons (<60 ps).[11] The simple application of 'pump-probe' techniques,[12] where the pump signal is synchronized with the x-ray bunch clock and its higher harmonics, provides a lower limit of several hundred MHz at most synchrotron facilities. Techniques have been developed to characterize pulsed dynamics at repetition rates less than the bunch frequency. To this end, Acremann *et al*. implemented a sophisticated software-defined photon counting system.[13] Due to the typically low incident photon flux (10^8ph/s), photon counting is the preferred acquisition mode in current STXMs.

We present a simpler differential photon counting approach for a moderate frequency regime. Using a commercial dual-gate photon counter for image acquisition we take, as the image basis, the difference between transmitted photon counts at high and low points on a modulating field cycle. Because the minimum gate width is 2 ns, low-frequency dynamics over a frequency range of 200 MHz to dc can be straightforwardly probed.

In this paper, we demonstrate this technique in the domain imaging of micron-size $Ni_{81}Fe_{19}$ ellipses with well-defined closure domain states. Different domain configurations were observed for identical sweep cycles during the static study. The stochastic nature of domain dynamics in these structures gives an explanation for the varied contrast observed in the differential images obtained at $\leq$2 kHz frequencies, with the best imaging found for small domain displacements.

II. EXPERIMENTAL TECHNIQUE

Two patterned structures, a single layer element and a bilayer element, were investigated. The preparation conditions were chosen to yield materials of optimal soft magnetic properties. A coercive field, $H_c < 1$ Oe, was seen in identically deposited unpatterned films at 16 Hz. For the first sample, a 15 nm layer of $Ni_{81}Fe_{19}$ (Permalloy) was deposited on a 200 nm Si_3N_4 membrane using UHV magnetron sputtering, with DC power of 200 W and an Ar pressure of 1.2 mTorr, at a deposition rate of 3.2 Å/s. 3 nm Ru was sputtered prior to the Permalloy as a seed layer to give better soft magnetic properties, and 10 nm MgO serves as a cap to protect the Permalloy from oxidation. Arrays of elliptical elements (5 $\mu m \times 12$ μ m) were fabricated using photolithography and a lift-off process. For the bilayer sample, the dimensions of the ellipse were changed to 5 $\mu m \times 24$ μm, and a sandwich structure of 15 nm Permalloy/5 nm Ru/15 nm Permalloy

a)Author to whom correspondence should be addressed. Electronic mail: cc3043@columbia.edu.

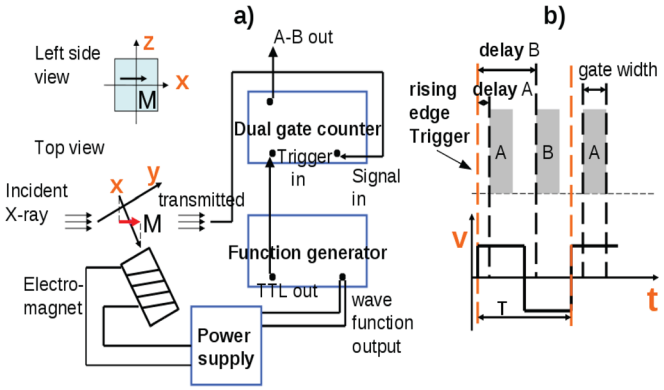

FIG. 1. (Color online) Experimental setup at CLS 10ID-1. (a) Configuration of the incident x-ray beam, sample plane, and photon detector; equipment setup for photon counter and function generator. (b) The wave function, trigger signal, and configurations for the 2 counting gates. See the text for details.

replaced the single 15 nm Permalloy layer, while the other conditions remained the same.

The scanning transmission x-ray microscopy (STXM) measurements were carried out at the Canadian Light Source (CLS), soft x-ray spectromicroscopy beamline 10ID-1 (SM), with the x-ray photon energy set to the Fe L_3 edge at 707 eV for the maximal x-ray magnetic circular dichroism (XMCD) signal.[15] The circular polarization of the incident x-rays is fixed during each image acquisition. Figure 1 shows the configuration of the experiment for the dynamic measurements. As illustrated in Fig. 1(a), the thin film element lies in the *xz* plane, with its normal pointing in the *y*-direction. The x-ray is propagating in the *xy* plane, 30° away from the sample plane normal. The projection of the element's in-plane magnetization onto the x-ray propagation direction contributes to the contrast at each pixel. The x-ray spot (40 nm at optimal focus) is scanned over the element to form an image.[11,16]

We used a commercial dual-gate photon counter with a minimum gate width of 2 ns to detect the transmitted x-ray intensity. During operation of the dual-gate photon counter, the number of photons detected over a time interval set by a gate width is counted, then integrated over a specified number of counting periods to give an adequate signal intensity. The starting point of the counting period is determined by a delay with respect to the trigger signal. To apply the magnetic fields, we used wound Cu coils of turn density $\sim$1-10 mm^{-1} with ferrite cores. The core material was tapered and positioned as close as possible to the sample stage of the STXM. The ferrite cores are rated for a flat frequency response to >1 MHz; ac fields were driven in a constant voltage mode (square wave) and calibrated by an ac Gauss probe as a function of frequency. The field values cited have a high ($\sim$50%) uncertainty between Figs. 4(a)–4(c) because the core was repositioned in each case and could not be calibrated *in situ*.

Figure 1(b) explains the temporal resolution. A function generator applies a square wave voltage to the coils of the ferrite-core electromagnet, exerting an alternating in-plane magnetic field to the element. The rising edge of the transistor-transistor logic (TTL) output from the function generator triggers the photon counting gates. The widths of the 2 photon counting gates, A and B, were both set to 1/5 of the square wave period, *T* (ms). The delay of gate A was set to 1/20 *T* while gate B lagged gate A by a half period. We took the images with 100 pixels in the *x*-direction and 25 pixels in the *z*-direction, respectively. The microscope dwelled at each pixel for 120 ms. The number of counting periods, *N*, for signal integration was thus set accordingly for each acquisition frequency, $N = 60/T$, to allow for 2 data points at each pixel. The differential signal, A-B, is then converted to an analog voltage and sent through a voltage-to-frequency converter before being recorded by the microscope.

For the static hysteresis loop measurements, we cycled the static field between −15 and +15 Oe along both axes of the single-layer ellipse. The STXM images with both x-ray helicities at each static field point were taken. Subtracting the 2 images in the software gives the differential contrast. The normalized magnetizations were obtained from the area ratio of the domains with the opposite contrasts (dark and bright).

III. RESULTS AND DISCUSSION

The static hysteresis loop was measured for the single-layer element in the horizontal configuration, with its short axis lying in the *z*-direction and the applied field in the *x*-axis. Figure 2 shows the remanent state. At the zero applied field, the element appeared to be in a well-defined 2-domain state with equal areas. Note that closure magnetization at the ends, if tangent to the boundary as expected, will show no contrast in this geometry. We cycled the sweeping field twice, starting from saturation at −12 Oe, increased the field to +12 Oe, and looped back to −12 Oe again to complete the cycle. Domain patterns at different field points during the first cycle are displayed in Fig. 3(a), showing the area change in the 2 domains. The overall hysteresis loop for the first cycle is shown in Fig. 3(b) as dots. During the second cycle, as represented on the loop by triangles, the element showed a different domain pattern as the applied field decreased from 12 Oe to 0 Oe. This behavior is shown in the upper panel of Fig. 3(c). In the lower panel, the element took a diamond pattern for zero net magnetization, instead of the 2-domain state.

The observed domain images, taken on the major loop, clearly show a stochastic component to the reversal behavior. The different states can be understood through the simulation results obtained by Hong *et al.*;[17] the domain configuration initiated in the *c-state* from saturation in the first cycle, and took the *s-state* in the second cycle. Due to the near-degeneracy in the lowest energy domain configurations, the same spot in the sample is likely to have opposite magnetization directions during different magnetization cycles from saturation. In dynamic measurements where the transmitted

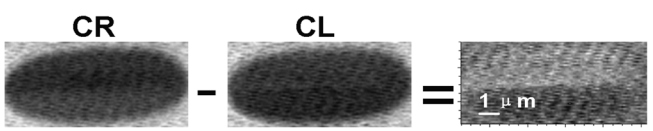

FIG. 2. The 5 μm × 12 μm element, static domain structure, at zero field, in the horizontal configuration. Here, CL denotes circular-left polarization, and CR denotes circular-right polarization; the XMCD image is on the right.

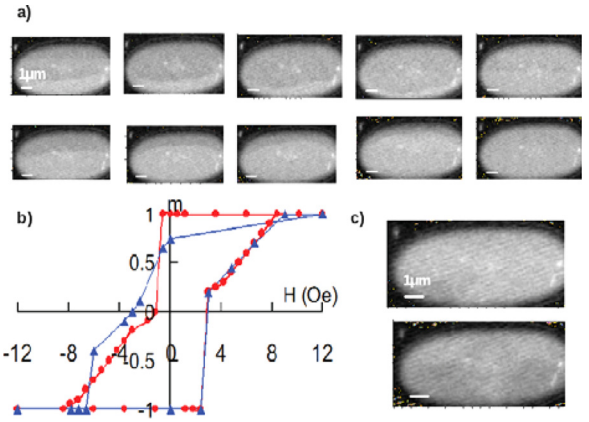

FIG. 3. (Color online) The 15 nm Permalloy ellipse static hysteresis loops; horizontal configuration. The bar equals 1 μm. (a) Field strengths from left to right are 3, 5.4, 7.2, 7.8, and 8.4 Oe; the opposite direction in the upper and lower panels. (b) Hysteresis loops by converting relative areas into normalized magnetization; the red curve (dots) denotes the first cycle; the blue curve (triangles) denotes the second cycle. (c) Different domain structures (diamond pattern) in the second cycle. Upper panel: 0 Oe; lower panel: −5.4 Oe.

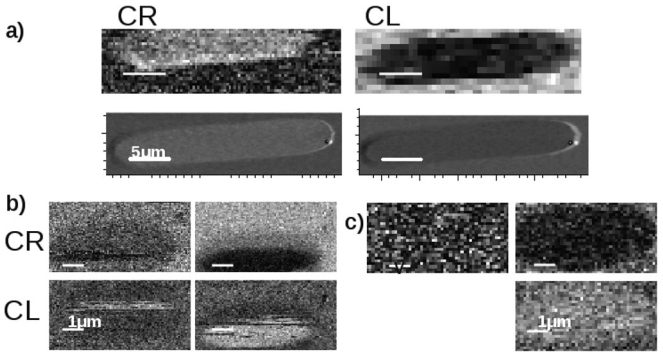

FIG. 4. Dynamic images; fields are estimated to 50% precision. (a) Bilayer 5 μm × 24 μm element; applied field 7 Oe along the long axis, fully switched. Upper panel: dynamic images, taken at 500 Hz; lower panel: static. (b) Horizontal configuration for the 15 nm × 5 μm × 12 μm element; applied field frequency is 500 Hz. As the field amplitude goes from 2 to 4 Oe, the switched area in the element grows. (c) Horizontal configuration for the single layer element at 2 kHz. The first column (field amplitude: 3.5 Oe) shows an example of no contrast due to the stochastic domain motion; the second column (field amplitude: 21 Oe) shows the contrast for the fully switched element.

photon counts are integrated over multiple cycles, inconsistency between cycles will lead to a reduction in the contrast, compared with static imaging.

Figure 4 demonstrates the dynamic images. In Fig. 4(a), the bilayer element is fully switched in a 500 Hz square wave external field, reversing at 7 Oe amplitude. The enhanced contrast is compared with the corresponding static XMCD images, acquired by subtracting two images taken at opposite bias field directions with the same x-ray polarization. When the element is not fully switched by the alternating external field during dynamic acquisitions, the area through which the domain wall moves during the cycle will show contrast. This area is expected to be roughly proportional to the applied field strength. The images in Fig. 4(b), taken at 500 Hz for the single layer element, show such a trend as the field is increased from left to right. In Fig. 4(c), the images were taken at 2 kHz. At the field amplitude 3.5 Oe, the picture shows no detectable contrast. We do not expect the dynamic coercivity to play a role at these sweep rates ($dH/dt < \sim 1 \times 10^4$ Oe/s); threshold rates have been measured in the range of $10^6 - 10^7$ Oe/s.[9] We attribute the relatively low contrast in Fig. 4(c) to stochastic effects along the major loop. When the field amplitude is 21 Oe, the fully switched element shows contrast.

In conclusion, we have demonstrated a new approach to time-resolved measurements in x-ray microscopy, which is not constrained by the bunch clock at synchrotron facilities. Implementing the concept of lock-in detection, the differential signal allows for contrast enhancement, provided that the process under investigation is reproducible over multiple cycles which are necessary for signal integration. The scope of this technique can also be extended to contrast enhancement in the precessional magnetization dynamics of nanostructures. Lock-in amplification of the transmitted diode intensity under RF field modulation has provided a 1-2 order of magnitude improvement in the signal detector in time-resolved XMCD.[14] When a differential signal is not required, any of the two gates can perform the regular photon counting at flexible rates and delays.

ACKNOWLEDGMENTS

We acknowledge the NSF Grant No. ECCS-0925829 for support.

[1]D. A. Allwood, G. Xiong, C. C. Faulkner, D. Atkinson, D. Petit, and R. P. Cowburn, Science **309**, 1688 (2005).
[2]C. Chappert, A. Fert, and F. N. Van Dau, Nature Mater. **6**, 813 (2007).
[3]S. S. P. Parkin, M. Hayashi, and L. Thomas, Science **320**, 190 (2008).
[4]A. Krasyuk, F. Wegelin, S. Nepijko, H. Elmers, G. Schonhense, M. Bolte, and C. Schneider, Phys. Rev. Lett. **95**, 207201 (2005).
[5]G. Woltersdorf and C. Back, Phys. Rev. Lett. **99**, 227207 (2007).
[6]L. Bocklage, B. Kruger, P. Fischer, and G. Meier, Phys. Rev. B **81**, 054404 (2010).
[7]D. S. Gardner, G. Schrom, F. Paillet, B. Jamieson, T. Karnik, and S. Borkar, IEEE Trans. Magn. **45**, 4760 (2009).
[8]R. Meere, T. O'Donnell, N. Wang, N. Achotte, S. Kulkarni, and S. C. O'Mathuna, IEEE Trans. Magn. **45**, 4234 (2009).
[9]C. Nistor, E. Faraggi, and J. L. Erskine, Phys. Rev. B **72**, 014404 (2005).
[10]S. Yang and J. L. Erskine, Phys. Rev. B **72**, 064433 (2005).
[11]P. Fischer, T. Eimuller, G. Schutz, P. Guttmann, G. Schmahl, K. Pruegl, and G. Bayreuther, J. Phys. D: Appl. Phys. **31**, 649 (1998).
[12]H. Stoll, A. Puzic, B van Waeyenberge, P. Fischer, J. Raabe, M. Buess, T. Haug, R. Hollinger, C. Back, D. Weiss, and G. Denbeaux, Appl. Phys. Lett. **84**, 3328 (2004).
[13]Y. Acremann, V. Chembrolu, J. P. Strachan, T. Tyliszczak, and J. Stohr, Rev. Sci. Instrum. **78**, 014702 (2007).
[14]D. A. Arena, Y. Ding, E. Vescovo, S. Zohar, Y. Guan, and W. E. Bailey, Rev. Sci. Instrum. **80**, 083903 (2009).
[15]G. Schutz, W. Wagner, W. Wilhelm, P. Kienle, R. Zeller, R. Frahm, and G. Materlik, Phys. Rev. Lett. **58**, 737 (1987).
[16]J. Stohr, Y. Wu, B. D. Hermsmeier, M. G. Samant, G. R. Harp, S. Koranda, D. Dunham, and B. P. Tonner, Science **259**, 658 (1993).
[17]B. Hong, T. Hayward, C. Barnes, and J. Jeong, IEEE Trans. Magn. **45**, 2511 (2009).